


Simulation of Urban Crash Occurrence Based on Real-World Crash Data

Transportation Research Record
2023, Vol. 2677(2) 1150–1164
© National Academy of Sciences:
Transportation Research Board 2022
Article reuse guidelines:
sagepub.com/journals-permissions
DOI: 10.1177/03611981221112400
journals.sagepub.com/home/trr


Marcel Langer¹ , Ronald Kates², and Klaus Bogenberger³ 

Abstract

The intelligent application of simulation is of central importance for the successful development and testing of automated driving functions. Realistic virtual environments are required to assess and optimize both the efficiency and safety of automated driving functions in real-world traffic situations. While existing traffic flow simulation frameworks excel at evaluating traffic efficiency, the implementation of human failure models and traffic safety aspects is a current field of research. In this publication, the occurrence of human failures is inferred from real-world crash statistics and introduced into traffic simulation. A realistic traffic simulation setup of the city of Ingolstadt, Germany, is used as a basis for this simulation of crash occurrence. Focusing on intersections as the most important urban crash hot spots, the relation between human failures and the occurrence of collisions is estimated for each conflict point in the simulation network. From crash statistics, the distributions of crash quantities and types across the intersections in the simulation network are calculated. An Iterative Proportional Fitting algorithm is used to project crash counts available at the intersection level onto the “conflict level,” determined by intersecting traffic streams within intersections. Human failures are generated and applied to traffic participants in the simulation using a Monte Carlo selection. The results demonstrate the functionality of the method for calibrating models for realistic crash occurrence in traffic simulation. This methodology provides a basis for simultaneous evaluation of both traffic efficiency and traffic safety impacts of future developments in urban traffic networks.

Keywords

pedestrians, bicycles, human factors, human factors of infrastructure design and operations, advanced driver assistance systems, driver performance, human factors in vehicle automation, safety, calibration, crash data, crash frequency, crash severity, modeling and forecasting, safety effects of connected/automated vehicles

Existing traffic flow simulation frameworks excel in evaluating the influence of infrastructure, regulation measures, and individual behavior on traffic efficiency. The underlying models are designed to simulate collision-free traffic. However, with the approaching introduction of automated vehicles into everyday traffic, a simultaneous evaluation of the tradeoff between traffic efficiency and traffic safety is becoming more and more relevant. Automated driving makes it possible to implement desired behavior directly into the vehicles. This enables the realization of driving strategies focused on long-term benefits to the entire traffic system. To ensure the potential of automated vehicles is utilized entirely, a simulative evaluation of the influence of their behavior on both traffic efficiency and traffic safety must be carried out.

In order to apply traffic simulation frameworks for the evaluation of traffic safety, the available literature

suggests adding human factors to the otherwise collision-free simulation models. Already in 2000, Archer and Kosonen (1) apply errors to the perception, decision making, and actions of drivers in a microsimulation tool. During the last decade, considerable research on the modelling of human factors in microscopic traffic simulation has occurred (2). A common approach is to randomly apply pre-defined human failures to existing microscopic models to generate safety-critical situations

¹AUDI AG, Ingolstadt, Germany

²REK Consulting, Otterfing, Germany

³Chair of Traffic Engineering and Control, Technical University of Munich, Munich, Germany

Corresponding Author:

Marcel Langer, marcel.langer@tum.de

and potentially collisions. Safety-critical situations are modelled by introducing speeding, slow driving, or abrupt stopping maneuvers into an Aimsun simulation, which were applied to a highway in Shanghai in Wang et al. (3). A similar approach is presented in Yang et al. (4) to evaluate collision avoidance systems for a platoon in which the lead vehicle sharply decelerates. Based on real-world traffic measurements on an urban motorway, Azevedo et al. (5) generate rear-end, lane-changing, and run-off-road collisions by adding a random component to the behavior models in simulation.

Another human failure process is described by Astarita and Giofré (6). The authors generate collisions in the simulation frameworks Aimsun and Vissim by modelling distracted drivers who move along a straight trajectory and potentially collide with other vehicles or roadside barriers. To evaluate the criticality of situations, they consider the collision energy in crashes and (for near misses) introduce a surrogate safety measure taking into account the proximity to roadside barriers. The relevance of surrogate measures to assess traffic safety is discussed in Young et al. (2), Pirdavani et al. (7), and Johnsson et al. (8). Astarita et al. (9) evaluate their previously presented surrogate safety measure as well as the entire simulation setup based on real-world crash data from nine intersections in Italy.

Further work has emphasized the capabilities of the human driver instead of applying random human failures. Human factors are introduced in traffic microsimulation by modelling the driver awareness dependent on the demand of the driving task in van Lint and Calvert (10). The presented model modifies a driver's reaction time and introduces perception errors into the car-following task dependent on the vehicle's environment and possible disturbing factors. The SEEV model ("Salience, Effort, Expectancy, Value"), presented in Wickens et al. (11), is another approach to modelling the occurrence of perception failures. The applicability of this model for the evaluation of human failures at urban intersections is evaluated in a driving simulator study in Werneke and Vollrath (12). Denk et al. (13) describe a concept of how this model could be applied to a stochastic traffic simulation.

Microscopic traffic simulation with integrated human factors is applied to evaluate advanced driver assistance systems by Yang et al. (4) and by Helmer (14). Helmer presents a stochastic simulation framework in which pedestrians cross in front of a vehicle equipped with a preventive pedestrian protection system. The severity of possible collisions is evaluated based on the impact speed and taken into account for the assessment of the driver assistance system. In order to assess the impact of automated driving systems on traffic safety, Rösener (15) simulates critical scenarios and collisions resulting from

cut-in situations on highways using a traffic setup from the simulation tool Vissim.

Crash data is used in Astarita et al. (9), Helmer (14), and Rösener (15) as an input to the presented simulation setups. Other simulation setups are based on surrogate safety measures obtained from real-world measurements (5, 7, 16, 17), or human factors are introduced entirely at random (4). However, the validation of simulation models predicting the impact of automated vehicles or other measures on crashes requires comparisons with real-world crash data. Based on naturalistic driving data, Khattak et al. (18) show that around 93% of all real-world crashes are caused by human failure processes, including both human errors and intentional violations of traffic regulation. The evaluation of crash data provided by Gerstenberger (19) suggests that this proportion is even higher at urban intersections, where only 3% of crashes with human injury result from environmental factors or technical defects. Therefore, since nearly all collisions at conflict points in urban intersections involve human failure processes, crash data can be evaluated to estimate what kind of human failure process leads to which number and type of crashes in which location. Joining the results of such an evaluation with exposure data (i.e., traffic volumes of different modes of participation), typically required for the setup of traffic simulations, can provide an estimation of the quantity of human failures that occur at different locations. Furthermore, by applying methods from crash research, the volatility of the data basis can be reduced to provide a more reliable basis for the simulation setup.

Methodology

In this publication, we present a calibration framework based on real-world crash data that applies human failures to an existing urban traffic simulation model. Since around 50% of urban crashes occur at intersections (7, 19), the focus lies on modelling crashes that result from traffic participants failing to yield the right of way while turning onto, crossing, or turning off a road at an intersection. The aim is to create a predictive simulation model for the evaluation of potential impact on urban traffic by automated driving or other interventions. This evaluation cannot be performed based solely on historical crash data. Due to redundancies in the traffic system resulting from infrastructure design and traffic control as well as the reactive behavior of traffic participants, not every occurrence of human failure (e.g., a red light or stop sign violation) results in a crash. However, this relationship between failure and crash may change with the introduction of automated vehicles—for example, due to modified traffic flow, speed distributions, and reaction times.

Therefore, in order to obtain a predictive simulation model, the occurrence of human failures is inferred from historical crash data using conflict analysis, statistical inference, and microscopic traffic simulation. The data flow and calibration procedure for this model are illustrated in Figure 1. Based on an existing urban traffic model of the city of Ingolstadt, Germany, real-world crash distributions for passenger cars and bicycles are reproduced across multiple crash types and all intersections of the simulation network. This framework has the potential to estimate the impact of automated driving or other interventions on urban traffic, assuming that the capability of human drivers and thus the incidence of human failures remain unchanged.

In the next section, we introduce the study area and collected data. Following this initial overview, the data flow and calibration procedure is presented as indicated by the corresponding numbers in Figure 1:

1. For the evaluation of simulated crashes, a crash severity model is required. We present suitable estimators for crash severity and introduce an established crash severity model by Müller et al. (20) to enable comparison between simulated and real-world crashes.
2. An open-source traffic simulation of the city of Ingolstadt (21), created based on the simulation framework SUMO (Simulation of Urban Mobility) (22), is introduced in the following section as a basis for the simulation of crash occurrence. The simulation incorporates the traffic demand of passenger cars as well as bicycles. Because of the particular relevance of car speeds for both the occurrence and severity of crashes, an accurate representation of the traffic speeds in the simulation is necessary for a realistic modeling of crash occurrence. Evaluations of crash statistics by Gerstenberger (19) suggest that speeding

plays a role in nearly 60% of crashes at urban intersections. The desired speeds of passenger cars in the simulation are therefore tuned to match real-world car trajectories using an adaptation of the method presented in Langer et al. (23).

3. Once the crash severity model and the simulation are set up, two crash databases are analyzed to obtain the input for the simulation of human failures. The first database, the *Unfallatlas*, contains all police-reported injury crashes in Germany for the years 2016 to 2020 (24). Since these crashes contain only high-level information of the crash type, the more detailed data from German in Depth Accident Study (GIDAS) (25) are analyzed to infer the distribution of different crash types across groups of similar intersections.
4. To generate car-to-car and car-to-bicycle collisions in the simulation, human failures are applied to both modes of participation via an external control script coupled to the simulation. Bicycle-to-bicycle crashes are not considered here.
5. Finally, the simulated crashes are compared to the real-world crashes in both location and type. An Iterative Proportional Fitting (IPF) algorithm is applied to determine a distribution of human failures in the simulation that best reproduces the real-world crash data. This projects the crash counts available at the intersection level as well as the crash type distributions onto the “conflict level”, determined by intersecting traffic streams within intersections.

The result of the proposed calibration method consists of a realistic traffic simulation coupled with a calibrated human failure model. The accuracy of this simulation setup for reproducing real-world crashes is assessed in the final section. By integrating automated vehicles into the setup or modifying infrastructure or traffic regulation,

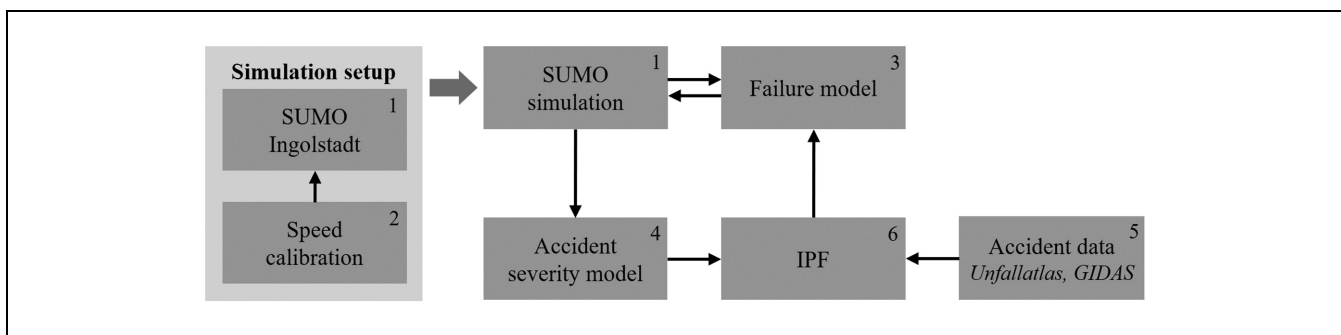


Figure 1. Methodology of the presented simulation setup.

Note: The simulation network is cropped from the open-source Simulation of Urban Mobility (SUMO) Ingolstadt simulation. An Iterative Proportional Fitting (IPF) algorithm is applied to project the real-world crash occurrence to the conflict points of intersecting traffic streams in simulation. The numbering in the figure refers to the corresponding detailed descriptions given in the main text.

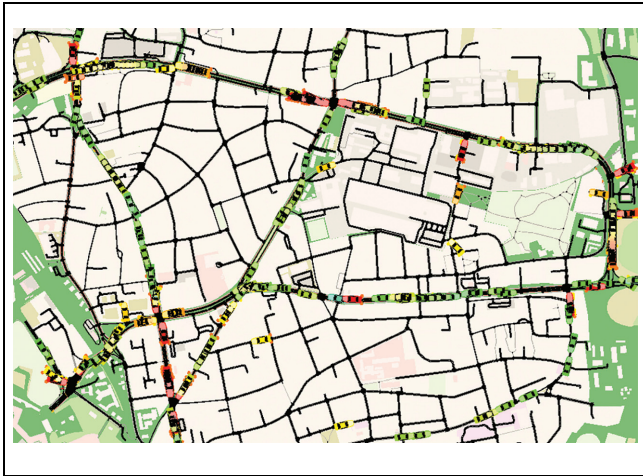


Figure 2. Study area as visualized in Simulation of Urban Mobility (SUMO).

the simulation can be employed to evaluate the impact of such measures on both traffic safety and efficiency in future applications.

Study Area and Collected Data

The presented simulation study is carried out in a road network spanning 5 km² in urban Ingolstadt. The area connects the Autobahn A9 to the city center and is made up mainly of residential districts with some office buildings as well as shopping and leisure facilities. The road network contains around 1,000 intersections, out of which 25 are signal controlled. The study area is visualized in the traffic simulation SUMO in Figure 2.

The following four types of data are available for the presented study:

1. Traffic demand data
2. Traffic light data
3. Car trajectory data
4. Historical crash data.

To determine the traffic demand in the study area, both statistical data as well as traffic counts are collected. The statistical data contains the distribution of inhabitants, work places, and shopping and leisure opportunities across the entire city and is provided by the city of Ingolstadt as well as Audi, as the major employer in the city. Furthermore, traffic counts are collected by induction loops at all traffic signals in the city. Together with these counts, the historical traffic light states are collected throughout the city and utilized to recreate the signal phases in the simulation. Based on this available data, the simulation is set up for passenger cars and bicycles as described later in the section “Simulation

Setup.” The traffic demand for an average weekday incorporates an estimated 121,000 trips of passenger cars and 8,500 bicycle trips, with up to 21,600 cars and 1,800 bicycles traversing the most frequented link per day.

Another real-world input for the traffic simulation is provided in the form of car trajectory data. The trajectories are collected via logging devices installed in cars in personal use throughout the city of Ingolstadt. The geo-location, heading, and speeds of the cars are measured by their built-in sensors and stored directly from their data buses. In total, over 100 h of data are available with a sample rate of 4 Hz. Using the geo-location and heading, the trajectories are matched to the links of the simulation network. The desired speeds of cars in SUMO are adjusted based on the map-matched real-world trajectories as described below.

As mentioned in “Methodology,” the crash data for the presented study is obtained from two different crash databases. The first database, the *Unfallatlas*, contains all police-reported injury crashes in Germany. It is provided by the German Statistical Offices for the years 2016 to 2020 as open data (24). Among other information, this data contains the geo-location of each crash, a high-level crash type, and a Boolean flag for each mode of transport involved in the crash. However, this database contains no attribution of which party was at fault. For the available time period, a total of 2,800 injury crashes are reported in the city of Ingolstadt. Within the presented study area, 188 intersection crashes are recorded and utilized for this study. A maximum of 20 crashes are reported at one of the major intersections in the network.

The second database, GIDAS, contains crashes recorded in the years 2000 to 2019 in the German cities Dresden and Hannover (25). This database can be evaluated to determine distributions of detailed crash types within the high-level crash types contained in the first database. Assuming that the distributions within the major crash types in the GIDAS crashes, recorded in Hannover and Dresden, are similar to those in Ingolstadt, the result of the data analysis is later employed to map the major crash types to the conflicts in the intersections. Furthermore, the GIDAS data can be evaluated to determine the at-fault mode type distributions. While car-to-car crashes are caused by either of the cars, crashes with bicycles involved can be caused either by the car or the cyclist, which must be modelled individually. Over 8,000 crashes from GIDAS are evaluated to determine the required distributions within the relevant high-level crash and mode types. Evaluations of the real-world crash data are presented below as a basis for the simulation of human failures.

The comparison with the presented injury crash data requires identification of likely injury crashes among all simulated crashes. The models used for this identification

are described in the following section. In particular, for car-to-car crashes, an established crash severity model is utilized.

Crash Severity Models

Crash severity models are required for the proposed simulation setup for two main reasons. Firstly, the most relevant improvement to traffic safety lies in a reduction of human injuries and fatalities. Therefore, when evaluating an automated driving system, besides the number of crashes that the system is involved in, the severity of the collisions that cannot be prevented must also be taken into account. Secondly, the safety simulation is created using two crash databases, which contain only injury crashes. Thus, to reproduce the real-world crash distributions, the likelihood of each simulated crash to produce injuries must be assessed.

Since both car-to-car and car-to-bicycle collisions are simulated, distinct models are required to predict the crash severity of these two crash types. According to literature, the severity of a car-to-bicycle collision can be predicted based on the impact speed of the involved parties (26, 27). While larger impact velocities generally lead to more severe injuries, there are multiple influencing factors, such as the point of impact of the cyclists on the car, which can lead to severe injuries even at lower speeds. Furthermore, an underestimation of minor injuries of cyclists must be expected, due to an underreporting of these crashes. For the simulation setup, we therefore assume that any car-to-bicycle collision above a speed of 5 km/h will result at least in a minor injury. The speed vectors of the involved parties in case of a collision can be obtained directly from the simulation.

For the assessment of the crash severity of car-to-car collisions, unlike for car-to-bicycle collisions, the impact speed of the involved cars is not a sufficiently accurate metric. Instead, the literature suggests that Δv , the reduction in speed resulting from the collision, is strongly correlated with the risk and severity of injuries (26, 28). Other than the impact speed, the Δv of cars involved in a collision cannot be obtained directly from the traffic simulation. In case of a full frontal collision of two cars with equal speed and mass, both cars would be decelerated to standstill and Δv would equal the impact speed. However, crashes resulting from turning maneuvers at urban intersections are particularly likely to involve cars colliding on different chassis parts with various velocities, angles, and overlaps. Therefore, a two-dimensional crash severity model presented by Müller et al. (20, 29) and Böhmländer et al. (30) is employed to calculate the Δv of cars involved in a collision.

In this crash severity model, two colliding cars are represented by masses and springs. The input to the model contains the two cars' masses, velocities, and headings. In

order to derive the force transferred between the cars in a specific crash constellation, the stiffness of the springs of each car must be tuned to accurately represent the properties of the cars' chassis in different areas of the body. This is achieved by training the model to reproduce the results of detailed finite-element-method (FEM) crash simulations. For the application in the traffic simulation environment, the model was set up to evaluate crashes between two identical Audi A3 cars with a mass of 1680 kg, length of 4.3 m, and width of 1.8 m. The resulting model is employed for the severity calculation of all simulated collisions. An improvement to the setup could be made by adding a distribution of different passenger cars of various shape and weight as well as trucks and busses with individual severity models to the simulation. However, in the presented initial setup, all simulated collisions between passenger cars are evaluated with the presented severity model.

A total of 338 FEM simulations containing a crash of two Audi A3 cars in various constellations are available for the calibration of the model. A random subset of 305 of these simulations is used to calibrate the mass-spring model, while the remaining 10% are set aside as test data. Comparing the calculated Δv for both cars between the mass-spring model and the FEM simulations shows a mean absolute error of 1 m/s on the training data and 1.1 m/s on the test data.

To simplify the simulation setup and enable a scalable architecture, the crash severity model is not connected directly to the traffic simulation. Instead, the model is employed to create a lookup table containing a Δv value for each car dependent on the first point of contact, the angle between the cars, and the car speeds. For this purpose, the two-dimensional shape of the Audi A3 chassis is approximated as a polygon made up of 23 points. The angle between the cars is modified in steps of 5° and the velocities of each car are varied between 0 m/s and 24 m/s in steps of 2 m/s. Each combination of the discrete contact points and velocities of each car as well as the angle between them leads to a possible collision constellation. Removing physically impossible constellations—for example, frontal collisions between cars moving in the same direction—yields a table with 600,000 collision constellations, which are calculated by the crash severity model. In Figure 3, exemplary Δv values from the table are depicted for frontal collisions and sideway collisions with different velocities and impact angles.

In order to compare the available crash statistics to the crashes in the simulation, the Δv values calculated by the severity model are combined with a probability for injury. Funk et al. (31) present evaluations of Δv values and injury severities for 228 crashes taken from the National Automotive Sampling System (NASS) database. Based on the presented probabilities for

human injury to result from crashes with different Δv values, the following linear injury risk function presented in Equation 1 is defined.

$$P(I) = \begin{cases} 0.16 \times \Delta v, & 0 < \Delta v \leq 2.7 \frac{m}{s} \\ 0.033 \times \Delta v + 0.34, & 2.7 \frac{m}{s} < \Delta v \leq 20 \frac{m}{s} \\ 1, & 20 \frac{m}{s} < \Delta v \end{cases} \quad (1)$$

For each car-to-car collision in the simulation, an interpolation is carried out to determine the initial point of contact based on the positions and velocities of both cars obtained from SUMO. The point on the polygon closest to this initial point of contact is calculated for each car and utilized together with the velocities and angles from simulation to select the corresponding Δv values from the lookup table. Finally, the probabilities for an injury to occur in either car are calculated from the Δv values following Equation 1. There are many other factors that influence the injury risk function such as the number of passengers in each car, the age of the passengers, and whether or not all passengers fastened their seatbelts. However, only the calculated Δv values are taken into account for the estimation of the crash severity in this publication.

Simulation Setup

An existing traffic simulation model of the city of Ingolstadt in SUMO is used as a basis for all further work. This simulation model is presented in Harth et al. (32) and available as open-source under TUM-VT (21).

It is set up with an accurate representation of the road network, traffic regulation, and traffic demand for passenger cars and bicycles. The road network is imported from OpenStreetMap and manually improved using aerial images available throughout the city. Many of the major links in the network have dedicated bicycle lanes, which are modelled following the road layout in the real world.

The traffic demand is initially modelled based on statistical data for the city of Ingolstadt introduced above. As described in Harth et al. (32), origin-destination matrices for passenger cars and bicycles are created from this data. The passenger car demand is further improved in accuracy using induction loop counts collected at all traffic signals in the city. In addition to the traffic demand, traffic light programs are modelled based on historical traffic light states collected throughout the city (32). The result is a realistic traffic signal control in simulation including protected and unprotected flows, which is essential for the modelling of urban crashes.

Since a simulation of crash occurrence requires considerable computational resources, this study is not carried out using the entire city-wide simulation. Instead, the road network of the previously presented study area is cropped from the large simulation network and used for all following analyses of traffic safety. The cropped simulation network is depicted in Figure 2. To ensure a realistic representation of the traffic demand in the smaller simulation, the routes for both modes are generated using the city-wide simulation and clipped at the fringes of the smaller network. For the following simulation of crash

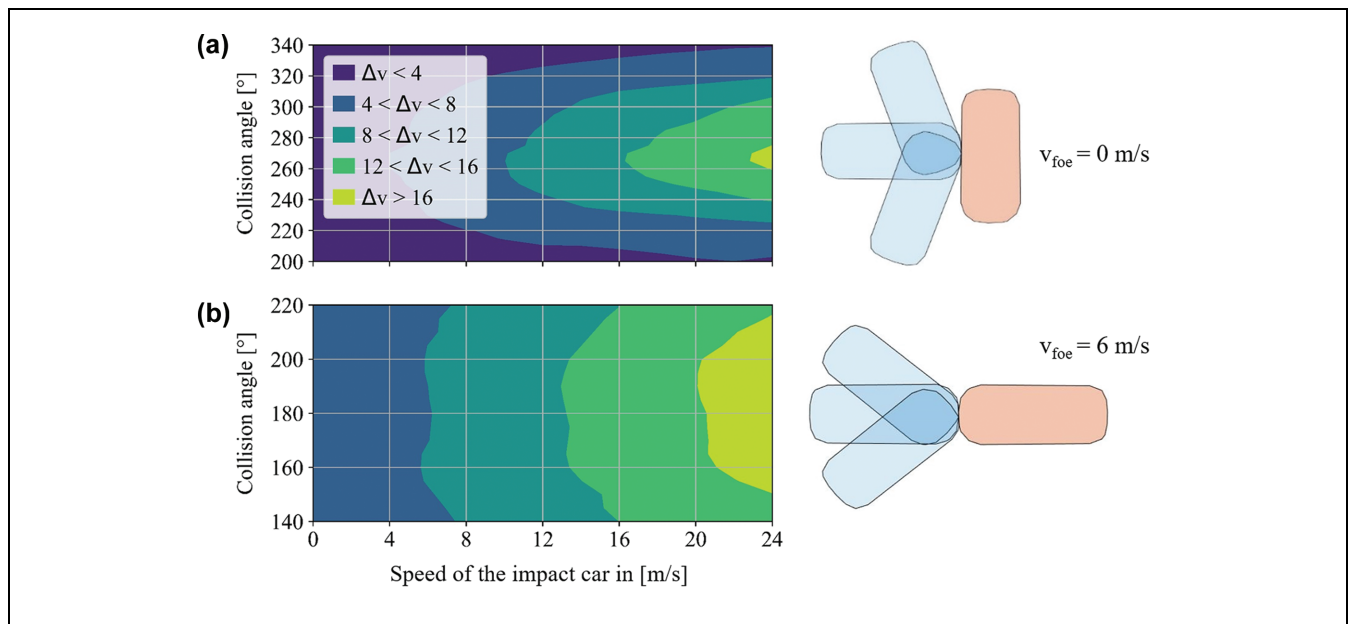


Figure 3. Exemplary Δv values calculated by the crash severity model for different velocities and angles of the impact car.

Note: The distributions for (a) sideways collisions and (b) frontal collisions are calculated for fixed positions and velocities of the foe car (v_{foe}). Δv denotes the reduction in speed of the impact car resulting from the crash.

occurrence, this simulation is run with a simulation time-step of 250 ms.

The simulation model is refined further using real-world car trajectory data. A realistic representation of the car speeds in traffic simulation is of major importance for a simulation of crash occurrence. The causal relation between traffic speeds and crash occurrence is a topic controversially discussed in the literature. Gitelman et al. (33) evaluate the relationship between injury crashes and the observed mean speed on rural single-carriageway roads in Israel. The results indicate that higher mean speeds generally lead to a larger number of injury crashes. In contrast, Pei et al. (34) show there can be a counterintuitive conclusion dependent on the employed method of aggregation and the exposure considered. The authors conclude that higher speeds lead to a higher crash risk when accounting for distance exposure, while the correlation is negative when considering time exposure. In a third study, Imprialou et al. (35) evaluate crashes over multiple road types. They come to the result, that crash risk increases up to a speed of around 85 km/h and decreases again above this speed.

The referenced publications discuss the general influence of traffic speeds on crash risk. However, it is clear that once a safety-critical situation arises, higher velocities make it more difficult for the involved parties to avoid a collision. Furthermore, as discussed in the previous section, in the case of a collision, higher speeds generally lead to more severe crashes. In order to simulate urban crashes accurately, it is therefore essential to model the speed distributions realistically in the traffic simulation.

Therefore, the desired speeds of cars in the simulation are calibrated with a method adapted from Langer et al. (23). For the links in the Ingolstadt SUMO network, real-world speed distributions are obtained by evaluating more than 100 h of real-world car trajectory data. For each link with more than 1 min of measurement data, the speed distributions are compared to the distributions in the simulation of an average weekday on an hourly basis. The simulation setup is assessed by calculating the deviation between the simulated and real-world speed distributions via the Kolmogorov–Smirnov test. This deviation is utilized as a fitness value for the optimization of the simulated speeds with a Genetic Algorithm (23).

However, it is concluded in Langer et al. (23) that assigning a city-wide factor to the desired speeds of simulated cars only insufficiently models the distribution of the desired speeds across roads with different properties. The Highway Capacity Manual (HCM) (36) suggests adjustment factors to car speeds—for example, for the number of lanes, lane width, median type, and lateral clearance of a road. The required inputs for two

influencing factors can be determined from the SUMO network: the number of lanes and the existence of an opposing lane. Therefore, the described method is adapted to calculate three parameters to define the desired speed:

$f_{overall}$: Overall factor for the desired speeds relative to the speed limit.

f_{lanes} : Factor for roads with more than one lane

$f_{opposing}$: Factor for roads without oncoming lanes (one-way or separated by median)

The mean desired speed per road is obtained from Equation 2. By default, SUMO draws the desired speed of each car from a normal distribution with standard deviation 10% of the speed limit around this mean value.

$$\overline{desired\ speed} = f_{overall} \times f_{lanes} \times f_{opposing} \times speed\ limit \quad (2)$$

The Genetic Algorithm is run for 15 iterations with a population size of 12. All adjustment factors are optimized in the range 0.9 to 1.2. The final results are $f_{overall} = 1.07$, $f_{lanes} = 1.06$, and $f_{opposing} = 1.04$, which is consistent with the HCM model. Multiple optimization runs converge to similar results in a range ± 0.01 . While the first factor is applied to the desired speed of each individual car, the two location-dependent factors are factored in to the edge-specific speed limits defined in the simulation network. This results in a desired speed with mean of 18% above the real-world speed limit for cars on median separated roads with at least two lanes per direction. However, cars in the simulation are regularly prevented from traveling at their desired speed by traffic lights, right-of-way regulations, or leading traffic participants. To determine the resulting speed increase in the simulation, the simulated average speeds on the selected links are compared before and after applying the factors described above. This evaluation shows that the increase of 18% for the desired speeds on the selected links leads to a 7.4% increase of the average speed from 37.9 km/h to 40.7 km/h.

Evaluation of Real-World Crash Data

In order to create a basis for comparing simulated and real-world crashes in Ingolstadt, two crash databases are evaluated. Here, the results obtained from the crash data are used as an input to the simulation based on the assumption that all injury crashes are reported to the police. Underreporting could be taken into account for recalibration by incorporating a city-wide, intersection-specific, or crash-type-specific underreporting model. As introduced above, the first database, the *Unfallatlas*,

contains the geo-location and the involved modes of transportation for all police-reported injury crashes. Furthermore, each crash is assigned a one-digit (major) crash type. These crash types are based on the more detailed three-digit crash types widely used in German crash research and defined by German Insurers Accident Research (37). The two major crash types that result from conflicts within intersections are types 2 and 3. The type 2 describes crashes resulting from conflicts between one traffic participant turning off a road and another participant traveling in either direction on the same road. Crashes of type 3 occur when a traffic participant fails to yield to a prioritized traffic stream while turning onto or crossing the prioritized road. The only crash type within intersections not represented in types 2 and 3 is one resulting from any kind of U-turn maneuver, which would be assigned the crash type 7. While other crash types can also occur within the geometric bounds of intersections, they do not result from conflicts between intersecting streams of traffic and are therefore not taken into account in the following sections. All further evaluations of crash data as well as the modelling of human failure is carried out for crashes of major types 2 and 3.

Out of the 2,800 crashes with human injury that were reported in Ingolstadt from 2016 to 2020, 20% were type 2 crashes, and 27% were assigned type 3. As described above, crashes of both major types can result from different types of conflicts dependent on the intersection geometry and traffic regulation. Therefore, the distribution of the detailed three-digit crash types among the two major crash types cannot be deduced from the first database. Furthermore, the described data contains no information on which party the main responsibility for crash was assigned to. Therefore, the more detailed GIDAS database (25) is evaluated to obtain distributions across the three-digit crash types and at-fault mode types. The crashes of major type 2, which can occur when turning off a road in SUMO, are presented in the following enumeration together with the corresponding three-digit crash types from the crash type catalogue (37):

1. Turning left without priority (crash types 211, 212, 213, 223, 224)
2. Turning left with priority assigned by a traffic signal (crash types 281, 283)
3. Turning right and yielding to a cyclist (crash types 243, 244).

Crashes resulting from right-turn maneuvers with priority at traffic signals or on priority roads whose direction changes are omitted from the evaluation, since neither of these intersection geometries are contained in the simulation network. All other crashes are not taken into account in the following simulation setup, since they

either involve mode types other than passenger cars and bicycles or result in a collision between cars in the same lane, which would require more detailed modelling of the longitudinal or lateral behavior of cars. Nonetheless, the presented crash types contain the most common crash types in the GIDAS data and represent 71% of all type 2 crashes. Similarly, the simulated type 3 crashes result from:

1. Conflicts with a prioritized traffic participant from the left (crash types 301, 302, 303, 304, 311, 312, 313, 314, 341, 343)
2. Conflicts with a prioritized traffic participant from the right (crash types 321, 322, 331, 332, 342, 344).

These represent 95% of all car-to-car and car-to-bicycle crashes in the evaluated GIDAS data. For the presented crash types, distributions are calculated from the GIDAS data. However, it must be expected that these distributions vary between intersections with different traffic regulation and geometric properties. Therefore, the distributions are calculated individually for groups of intersections with similar properties. An assessment of which properties influence the occurrence of different crash types can be obtained from literature. The results presented by Wang et al. (38) indicate that the intersection shape, complexity, and traffic volumes as well as the gradient and speed limit of incoming roads have a measurable influence on crash occurrence. This aligns mostly with a publication by Gomes et al. (39), who add the traffic regulation (signalized, stop-controlled, yield, right-before-left) to the list of relevant intersection properties. In a further publication, Gitelman et al. (33) agree with the importance of traffic volumes and the speed limit for estimating crash occurrence but mention the curvature, shoulder width, and median type of incoming roads as well. From the results of the literature review, we select intersection properties, which can be accurately obtained for the crashes from both databases as well as for the intersections in the simulation network. The following Boolean classifications are defined to split intersections into eight possible groups:

1. Traffic light regulated (yes versus no)
2. Number of legs (< 4 versus ≥ 4)
3. Maximum speed limit on incoming legs (≥ 50 versus < 50 km/h)

Since there are no signalized intersections with a speed limit below 50 km/h in the aforementioned simulation network, six groups of intersections remain for further evaluation. The distributions across these groups in the

Regulation	Legs	Speed limit	Crash type 2									Crash type 3											
			Minor p ₁			Major p ₂			Left without priority			Right without priority			Left with priority			From left			From right		
			Car	Car	Bike	Car	Bike	Car	Car	Bike	Car	Bike	Car	Car	Bike	Car	Bike	Car	Car	Bike	Car	Bike	Car
		30	1,00	0,53	0,12	0,00	0,35	0,00	0,00	0,00	0,00	0,00	0,00	0,00	0,00	0,42	0,14	0,07	0,58	0,50	0,29		
		50	1,00	0,49	0,01	0,00	0,49	0,01	0,00	0,00	0,00	0,00	0,00	0,00	0,00	0,83	0,32	0,05	0,17	0,59	0,04		
		30	1,00	0,68	0,07	0,00	0,25	0,00	0,00	0,00	0,00	0,00	0,00	0,00	0,22	0,13	0,05	0,78	0,30	0,52			
		50	1,00	0,62	0,08	0,00	0,29	0,01	0,00	0,00	0,00	0,00	0,00	0,00	0,60	0,33	0,08	0,40	0,49	0,10			
		50	0,87	0,42	0,03	0,00	0,47	0,08	0,13	0,00	0,00	0,00	0,00	0,41	0,21	0,16	0,59	0,45	0,18				
		50	0,88	0,33	0,04	0,00	0,58	0,03	0,12	0,01	0,01	0,00	0,00	0,44	0,15	0,24	0,56	0,33	0,28				

Figure 4. Distributions across the relevant crash types and at-fault mode type obtained from the German in Depth Accident Study (GIDAS) database.

Note: The columns indicate the crash types and the modes of participation. The at-fault participant p₁ approaches from the minor link while the involved participant p₂ is traveling on the major link.

over 8,000 evaluated GIDAS crashes are presented in Figure 4.

From the first crash database, it is determined how many crashes of each major type occur between cars and between cars and bicycles. Using the GIDAS evaluations presented Figure 4, it can be estimated how these crashes are distributed across the more detailed crash types introduced above. For example, at signalized, four-legged intersections (last row), 88% of the evaluated car-to-car crashes with major type 2 are *left-without-priority* crashes, while 12% are *left-with-priority* crashes. The portion for *right-without-priority* crashes between two passenger cars is zero, since this type always involves bicycles. Similarly, *left-with-priority* crashes can only occur at signalized intersections. Car-to-bicycle crashes are classified further depending on which mode type caused the crash. For example, 33% of type 2 crashes involving bicycles at signalized, four-legged intersections (last row) are of type *left-without-priority* and are caused by the car, while 4% are of the same type but caused by the cyclist.

The presented proportions of crash types *t* within the major crash types *T* of each group *g* and each mode of the at-fault participant *p*₁ and involved participant *p*₂ presented in Equation 3 are used as one input for the simulation.

$$f_{t,g,p_1,p_2} = \frac{A_{t,g,p_1,p_2}^{GIDAS}}{A_{T,g,p_1,p_2}^{GIDAS}} = \frac{A_{t,g,p_1,p_2}^{IN}}{A_{T,g,p_1,p_2}^{IN}} \quad (3)$$

The other input, the number of crashes *A*_{*T*,*b*}(*j*) per intersection *j*, major type *T* and bicycle involvement *b* (1 if bicycle involved, 0 if only cars), can be inferred directly from the map-matched crash database. However, in the 5 years of available data, 188 type 2 and 3 crashes were reported for the nearly 500 intersections of the cropped simulation network. A large number of intersections show zero reported crashes, and only 36 have more than

one. Due to the stochastic nature of traffic crashes, it cannot be assumed that the absolute number of crashes per intersection directly indicates the probability for crash occurrence in a given time period. Therefore, the Empirical Bayes (EB) method of crash research is applied. A comprehensible explanation of the EB method is provided by Hauer et al. (40). The EB method is used in crash research to calculate a more representative crash probability combining observations with an “expectation.” EB is applied to this challenge using the observed crash rate at each intersection as well as an expected crash rate across similar intersections. To calculate the “expected value,” the previously described groups of intersections with similar regulation, number of legs, and speed limit are utilized. To account for the different traffic volumes that pass each intersection, EB is applied to the crash rates instead of the absolute crash counts. For each major crash type *T* and bicycle involvement *b*, the crash rates *A*_{*T*, *b*, *rel*} per intersection *j* are calculated from the absolute crash count *A*_{*T*, *b*} and the traffic volumes *n*. The traffic volumes per intersection are set to the average daily car traffic for car-to-car crashes and to the daily bicycle traffic for car-to-bicycle crashes. Both volumes are obtained from the calibrated traffic simulation in SUMO (32). The expected group crash rate $\bar{A}_{T,b,rel}(g)$ is the mean crash rate within the group. Following the descriptions of Hauer et al. (40) and Elvik (41), the EB estimates for each intersection are calculated according to Equation 4.

$$A_{T,b,rel}(j|g) = \alpha \times A_{T,b,rel}(j) + (1 - \alpha) \times \bar{A}_{T,b,rel}(g) \quad (4)$$

$$\alpha = \frac{1}{1 + \frac{var(A_{T,b}(g))}{A_{T,b}(g)}} \text{ and } A_{T,b,rel}(j) = \frac{A_{T,b}(j)}{n(j)}$$

The parameter α is calculated here using the variance and mean number of crashes across all intersections in the group. Using the traffic volumes, the expected

number of crashes for the observed time period is calculated from the EB estimated crash rate and utilized as an input for the simulation.

Implementation of Human Failures

To generate collisions in the traffic simulation, human failures are applied to a portion of the traffic participants when approaching an intersection. As discussed in the introduction and presented by, for example, Khattak et al. (18), traffic crashes are caused by a wide range of human failures. However, for the presented simulation setup, each of the previously described crash types is modelled as a violation of the right of way within an intersection due to human error. A perception error is applied to participants approaching an intersection from the minor link, which makes the behavior model conclude mistakenly that it is safe to proceed through the intersection. To generate entering, crossing, and protected-left crashes at signalized intersections, the at-fault participant ignores the traffic signal as well. This procedure aims to produce more realistic behavior than creating entirely unaware simulated participants, since these would simply ignore streams of multiple prioritized participants and burst through dense traffic.

In order to implement this model of human failures, each geometric conflict point c in each intersection is mapped to the crash types using the definitions of straight, left, and right maneuvers as well as the right-of-way properties provided in the SUMO net file. For example, a conflict point at which a left-turning car crosses oncoming traffic will be mapped to either of the crash types *left-with-priority* or *left-without-priority* dependent on the traffic regulation.

The aim of the following calibration procedure is to estimate a probability for error occurrence at each conflict point (denoted as c) so that the simulation setup reproduces the real-world crash distributions in both type and location. This probability $P(E_{c,p_1,p_2})$ for one mode of participation p_1 on the minor link to overlook a single approaching prioritized mode of participation p_2 is defined for each conflict point c in each intersection of the simulation network. Based on this probability, perception errors are applied by an external control script in Python connected to the simulation via the Traffic Control Interface provided in the SUMO framework.

Another key aspect of simulating crash occurrence at urban intersections is modelling the reaction of the prioritized traffic participant to the impeding participant. Firstly, it must be ensured that the prioritized traffic participant realizes their right-of-way is being violated and triggers a realistic reaction in the simulation. This reaction is implemented in SUMO as described in Erdmann and Krajzewicz (42) and in the SUMO documentation.

Traffic participants in SUMO may become “impatient” when waiting at an intersection for a gap in the prioritized stream of traffic. At maximum impatience, a participant will enter the prioritized road even if this requires a prioritized participant to brake with maximum deceleration. However, participants will never impede prioritized traffic if the gap is too small for it to react in time. By implementing human failures as described above, this reaction is stressed to the point at which a collision is unavoidable.

To restrict the reaction to a realistic limit, the maximum deceleration is set to -7.5 m/s^2 for passenger cars and -7 m/s^2 for bicycles as suggested in the SUMO documentation. The only possible maneuver for both cars and cyclists to avoid collisions is braking with their maximum possible deceleration. Implementing evasive maneuvers for collision avoidance is not expected to provide a major improvement to the proposed setup. Evaluations of crash data by Gerstenberger (19) show that braking is the most common process in crash avoidance at intersections. Moreover, driving physics suggest that swerving for collision avoidance is unlikely to provide a significant advantage over braking at the low speeds in urban intersection traffic (43). Since no evasive maneuvers are implemented, all crashes are simulated as collisions between two traffic participants. Real-world crashes of major types 2 and 3 could result in single-sided collisions with roadside objects or vegetation if either participant is run off the road while trying to evade a conflicting participant.

Furthermore, the reaction of the prioritized participant is modelled taking into account human reaction times. By default, SUMO calculates the behavior of every participant in every simulation step. In the following setup, the simulation step length is set to 0.25 s. However, according to Green (44) for unexpected stimuli, a gamma distribution with mean 1.5 s would be appropriate for drawing reaction times. SUMO allows modelling delayed reactions by setting the action step length to a multiple of the simulation step length and thus update the participants only in specific simulation steps. By setting the action step length to 2 s, this leads to an even distribution across reaction times of 0.25 to 2 s. Applying an exact delay to the reaction in a critical situation would require more detailed modelling of the exact moment in which the prioritized participant realizes that braking is required as well as an overriding of the SUMO behavior via an external control script.

Failure Distributions Inferred From Crash Data

In order to reproduce the real-world crash distributions, a probability $P(E_{c,p_1,p_2})$ for the occurrence of human

error must be defined for each conflict point in the simulation. The probability for a crash to occur at a conflict point within an intersection can be described by the law of total probability, taking into account the probability $P(N_{c,p_1,p_2})$ for no error.

$$P(A_{c,p_1,p_2}) = P(A_{c,p_1,p_2}|E_{c,p_1,p_2}) \times P(E_{c,p_1,p_2}) + P(A_{c,p_1,p_2}|N_{c,p_1,p_2}) \times P(N_{c,p_1,p_2}) \quad (5)$$

We assume here that crashes result only from human errors. Therefore, the probability for a crash to occur without intervention of the error model $P(A_{c,p_1,p_2}|N_{c,p_1,p_2})$ is zero. In the following process, only collisions caused by the error model are evaluated, leading to the following probability for crashes:

$$P(A_{c,p_1,p_2}) = P(A_{c,p_1,p_2}|E_{c,p_1,p_2}) \times P(E_{c,p_1,p_2}) \quad (6)$$

The probability for an error to result in a crash $P(A_{c,p_1,p_2}|E_{c,p_1,p_2})$ is dependent on the geometry of the conflicting links as well as the traffic volume of participants p_2 on the prioritized link. The frequency of crashes at conflict point c results from the probability for crash multiplied by the traffic volume n_{p_1} of the minor link.

$$\hat{A}_{c,p_1,p_2} = P(A_{c,p_1,p_2}|E_{c,p_1,p_2}) \times P(E_{c,p_1,p_2}) \times n_{c,p_1} \Leftrightarrow P(A_{c,p_1,p_2}|E_{c,p_1,p_2}) = \frac{\hat{A}_{c,p_1,p_2}}{P(E_{c,p_1,p_2}) \times n_{c,p_1}} \quad (7)$$

In order to determine $P(A_{c,p_1,p_2}|E_{c,p_1,p_2})$, multiple simulations are run with an equal error probability of $P(E_{c,p_1,p_2}) = 0.1$ across all conflict points. With this error probability, an Adaptive Importance Sampling simulation is set up, in which large numbers of crashes are simulated within a minimal simulation duration. By determining the probability for a crash to result from an error $P(A_{c,p_1,p_2}|E_{c,p_1,p_2})$ at a specific conflict point, we can later tune the probability for an error to occur $P(E_{c,p_1,p_2})$ to reproduce the real-world crash counts. Therefore, the number of crashes resulting at each conflict point in simulation S_{c,p_1,p_2} is measured for $P(E_{c,p_1,p_2}) = 0.1$ fixed across all conflict points. Since no more than one perception error is applied to each participant per intersection, the conflicts are separated by the crash types as well as by the involved parties. Whether a perception error leads to a crash depends on the volume, speed, and reaction time of the prioritized traffic as well as the intersection regulation and geometries. The crash frequencies are simulated for the five crash types t and three possible involvements of passenger cars and bicycles. To obtain these 15 crash frequencies, an average weekday is simulated multiple times to provide reliable

results and account for the stochastic variance between the simulation runs. For the following results, each crash frequency is estimated in 60 simulated days, which represents an acceptable trade-off between accuracy of the estimation and computational effort. Traffic volumes and traffic signals are modelled throughout the day based on real-world data as previously described in the simulation setup. These 900 days of simulation are run 30 in parallel on a local simulation cluster to keep the computation time in a feasible range. Before each simulation run, the departure times of all cars are shuffled within each hour of the day, and the random seed in SUMO is modified to introduce stochastic variance to the conflict situations occurring in the simulation. Using this realistic traffic simulation setup, the probability for a crash to result from an error is estimated following Equation 8.

$$P(A_{c,p_1,p_2}|E_{c,p_1,p_2}) = \frac{S_{c,p_1,p_2}}{0.1 \times n_{c,p_1,60}} \quad (8)$$

It is the aim of our work to reproduce the real-world crash occurrence in both type and location in the traffic simulation. Equations 7 and 8 can be utilized together to calculate which error probability would have to be set at each conflict point to produce an expected number of crashes in a specified duration of the simulation. However, the expected frequency of crashes per conflict point cannot be obtained directly from the crash databases. Instead, the frequency of crashes is known for each intersection $A_{T,b}(j)$ for both major types T and both variants of bicycle involvement b using the EB method. Each major crash type T comprises multiple detailed crash types t which can again result from multiple conflicts c between intersecting streams as described in Equation 9.

$$A_{T,b}(j) = \sum_{t \in T} \sum_{c \in t} A_{c,b}(j) \quad (9)$$

For example, crashes of major type 2 are made up of the three detailed types *left-without-priority*, *right-without-priority*, and *left-with-priority* as described in the previous section. Furthermore, each of these crash types can occur at multiple conflict points dependent on intersection geometry and regulation. For example, at a basic unsignalized four-way intersection, there will be four conflict points at which left turning cars yield to oncoming traffic and crashes of type *left-without-priority* can occur. Therefore, the previously presented evaluations from the GIDAS database are employed as a second input to the simulation setup. Following Equation 3, the global proportions of crashes, A_t , attributable to the more detailed crash types t for each major type T , can be inferred.

$$f_{t,g,p_1,p_2} = \frac{A_{t,p_1,p_2}}{A_{T,p_1,p_2}} = \frac{\sum_j \sum_{c \in t} A_{c,p_1,p_2}(j)}{\sum_j \sum_{t \in T} A_{c,p_1,p_2}(j)} \Leftrightarrow f_{t,g,p_1,p_2} \times \sum_j \sum_{t \in T} A_{c,p_1,p_2}(j) = \sum_j \sum_{c \in t} A_{c,p_1,p_2}(j) \quad (10)$$

This input from Equations 9 and 10 result in an underdetermined linear system. Firstly, only the global distributions of detailed crash type t instead of the distributions per intersection can be obtained from the GIDAS evaluation. Secondly, there exists no information on the distribution of crashes at the conflict level—that is, across the conflict points per intersection. In order to find a deterministic solution for this system, an additional modelling assumption on the distribution of crash occurrence across the individual conflict points is required. It would be unrealistic to assume equal distributions of crash types t within all intersections, because both the geometries and the traffic exposure of conflicting streams vary among the intersections. Instead, it is assumed here that the probability for an error to occur $P(E_{c,p_1,p_2})$ is equal for all conflicts per detailed crash type t . Based on this assumption, the distribution of crash frequencies across all conflict points and participations results from Equations 7 and 8.

$$\hat{A}_{c,p_1,p_2} = \frac{S_{c,p_1,p_2}}{0.1} \times \frac{n_{c,p_1}}{n_{c,p_1,60}} \times P(E_{c,p_1,p_2}) \quad (11)$$

As shown in Equation 11, the expected number of crashes per simulated day can be calculated for each conflict location directly from the error probability. However, this is only an initial crash distribution, which does not yet represent the inputs from Equations 9 and 10. Therefore, an IPF algorithm is applied in order to fit the simulated crash distributions to the real-world inputs. A detailed description of the IPF algorithm is provided by Idel (45). The IPF calculates a distribution of error probabilities across the conflict points, which is closest to the initial assumption while fulfilling the constraints given by Equations 9 and 10. This produces a distribution of crashes that considers the traffic volumes of participants p_1 and p_2 at each conflict point, as these are factored in with the simulated crash frequency S_{c,p_1,p_2} . Although the input to the IPF contains an even distribution of error probabilities across all conflict points, the final calibration output specifies individual probabilities that best reproduce the real-world crash statistics.

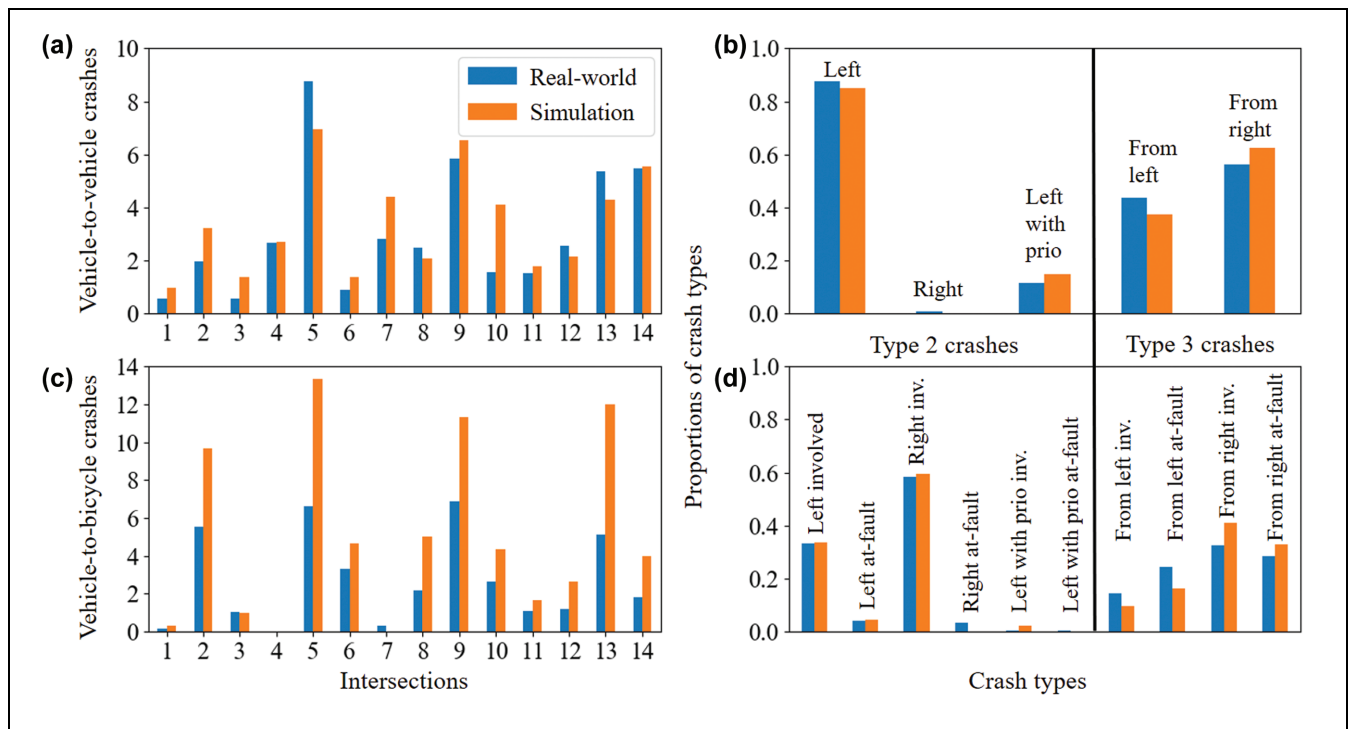


Figure 5. Results of final simulation setup for traffic light controlled four-legged intersections. Real-world crashes between 2016 to 2020 (blue) are reproduced in 60 days of simulation (orange): (a) and (b) car-to-car crashes; (c) and (d) car-to-bicycle crashes, classified also by at-fault party.

Note: The constellation “at-fault” versus “involved” refers to the cyclist.

Simulation Results

Using the IPF, the error probabilities are estimated to reproduce the real-world crash counts from 2016 to 2020 in 60 simulated days. In Figure 5, the results are assessed by comparison of simulation with both real-world data sources: crashes per intersection (left panels) and distribution of crash types t across the two major crash types (right panel). The results are obtained in three simulation runs with 60 days each for the 14 intersections of the sixth group (signalized, four-legged, speed limit 50 km/h).

These results for one of the intersection groups demonstrate the functionality of the presented method. Crashes are more likely to occur at intersections in simulation that also show higher crash rates in the real-world data. Model residuals, especially for the crash counts per intersection, reflect the stochastic nature of crash occurrence including the statistical variance of crash rates in simulation, which depend on computing resources. A second origin for the residuals concerns the simulative estimation of $P(A_{c,p_1,p_2}|E_{c,p_1,p_2})$. For the presented simulation, this is obtained from 60 days of simulation per crash type and modes of participation. For simulated conflict points in the high traffic intersections in group six shown in Figure 5, the defined error probability of 0.1 produces up to 600 crashes S_{c,p_1,p_2} in 60 days. However, at some conflict points, far fewer crashes are produced for the same error probability, which reduces the accuracy of the estimation. Because the number of conflicts scales bilinearly (i.e., linearly with both intersecting traffic volumes), these effects are pronounced at minor intersections with low traffic volumes. The crashes in intersections of the fifth group (signalized, three-legged, speed limit 50 km/h) are reproduced in number and type with similar accuracy as the results depicted in Figure 5, since the intersections of both groups have some of the highest traffic volumes in the simulation network. However, especially within the less frequented intersections of the other groups, deviations between the number of real-world and simulated crashes remain after the calibration procedure. At some conflict points in these intersections, zero crashes or only one crash were produced in the calibration, which impacts the IPF estimate. These issues could be addressed by increasing the computational effort in future applications of the methodology.

Conclusions and Outlook

Human errors and other failure processes are common in daily traffic. However, infrastructure design and traffic control, as well as the reactive behavior of one traffic participant to the failures of another, create a traffic system that is remarkably failure-tolerant and contains a high level of natural redundancies. The consequences of

human failures depend strongly on the dynamics of traffic and interactions of the involved parties. Therefore, we have presented a simulative approach, in which traffic simulation is employed to provide the traffic infrastructure, regulation, and demand as a basis for a simulation of urban traffic safety. By applying human errors to individual cars, the probability for a crash to result from an error was estimated and utilized to reproduce the real-world crash occurrence in the simulation. The presented method is applicable to any SUMO simulation with realistic traffic demand in which the expected number of crashes per intersection can be determined. While the overall method for adding human failure processes based on real-world crash data can be applied to any traffic simulation tool, the suitability of the built-in intersection simulation models must be evaluated individually.

Validation of simulation models predicting the impact of automated vehicles or other measures on crashes requires comparisons with real-world crash data, particularly in number, type, and severity. To this end, in this publication, the potential of reproducing real-world crash distributions in traffic network simulation while also quantifying traffic efficiency was demonstrated. This capability represents the key requirement for comprehensive assessment of novel influences such as automated driving on traffic networks. As an initial approach, automated vehicles can be incorporated into the simulation—for example, with lower reaction times and strict speed discipline using behavior models provided in SUMO. Based on this simulation of mixed traffic, an estimation of the impact of automated vehicles on urban traffic safety and efficiency can be made. Ultimately, precise algorithms for sensing, decision making, and trajectory planning of automated vehicles must be integrated to obtain accurate benefit estimates.

More detailed results based on larger quantities of simulated data and other refinements will be presented in following publications together with an application of the simulation setup for large-scale virtual assessment of the influence of the behavior of automated vehicles. Further improvements to the simulation setup could be introduced by modelling the influence of the time of day or environmental factors on error occurrence and human reactions. Furthermore, detailed evaluations of speed profiles, intersection crossing times, and the reactive behavior with introduction of the failure model could be carried out in addition to the comparison of crash numbers and types. More refined models of human failure processes are expected to improve the realism of the simulation setup.

Acknowledgments

The authors thank Marcus Mueller and Dennis Boehmlaender of AUDI AG for their support regarding the crash severity

model. Furthermore, we thank Markus Koebe of the Audi Accident Research Unit (AARU) for his support in the crash data evaluation.

Author Contributions

The authors confirm contribution to the paper as follows: study conception and design: M. Langer, R. Kates, K. Bogenberger; data collection: M. Langer; analysis and interpretation of results: M. Langer, R. Kates; draft manuscript preparation: M. Langer, R. Kates. All authors reviewed the results and approved the final version of the manuscript.


Declaration of Conflicting Interests


The author(s) declared no potential conflicts of interest with respect to the research, authorship, and/or publication of this article.

Funding

The author(s) disclosed receipt of the following financial support for the research, authorship, and/or publication of this article: This work is supported by the German Federal Ministry of Transport and Digital Infrastructure (BMVI) within the Automated and Connected Driving funding program under Grant No. 01MM2001 (SAVeNoW).

ORCID iDs

Marcel Langer  <https://orcid.org/0000-0003-3109-7821>

Klaus Bogenberger  <https://orcid.org/0000-0003-3868-9571>

References

1. Archer, J., and I. Kosonen. The Potential of Micro-Simulation Modelling in Relation to Traffic Safety Assessment. *Proc., ESS Conference*, Hamburg, July, 2000.
2. Young, W., A. Sobhani, M. G. Lenné, and M. Sarvi. Simulation of Safety: A Review of the State of the Art in Road Safety Simulation Modelling. *Accident Analysis and Prevention*, Vol. 66, 2014, pp. 89–103.
3. Wang, J., Y. Kong, T. Fu, and J. Stipanovic. The Impact of Vehicle Moving Violations and Freeway Traffic Flow on Crash Risk: An Application of Plugin Development for Microsimulation. *PLoS One*, Vol. 12, No. 9, 2017, pp. 1–22.
4. Yang, Z., X. Wang, X. Pei, S. Feng, D. Wang, J. Wang, and S. C. Wong. Longitudinal Safety Analysis for Heterogeneous Platoon of Automated and Human Vehicles. *Proc., Conference on Intelligent Transportation Systems*, Maui, HI, 2018, pp. 3300–3305.
5. Azevedo, C. L., J. L. Cardoso, and M. E. Ben-Akiva. Probabilistic Safety Analysis Using Traffic Microscopic Simulation. *arXiv Preprint arXiv:1810.04776*, 2018, pp. 2011–2014.
6. Astarita, V., and V. P. Giofré. From Traffic Conflict Simulation to Traffic Crash Simulation: Introducing Traffic Safety Indicators Based on the Explicit Simulation of Potential Driver Errors. *Simulation Modelling Practice and Theory*, Vol. 94, 2019, pp. 215–236.
7. Pirdavani, A., T. Brijs, T. Bellemans, and G. Wets. A Simulation-Based Traffic Safety Evaluation of Signalized Intersections. *Proc., 15th International Conference Road Safety on Four Continents*, Abu Dhabi, United Arab Emirates, March 28–30, 2010, pp. 1229–1239.
8. Johnsson, C., A. Laureshyn, and C. Dágostino. Validation of Surrogate Measures of Safety With a Focus on Bicycle–Motor Vehicle Interactions. *Accident Analysis and Prevention*, Vol. 153, 2021, p. 106037.
9. Astarita, V., C. Caliendo, V. Pasquale, and I. Russo. Surrogate Safety Measures From Traffic Simulation: Validation of Safety Indicators With Intersection Traffic Crash Data. *Sustainability (Switzerland)*, Vol. 12, No. 17, 2020, pp. 1–20.
10. van Lint, J. W. C., and S. C. Calvert. A Generic Multi-Level Framework for Microscopic Traffic Simulation—Theory and an Example Case in Modelling Driver Distraction. *Transportation Research Part B: Methodological*, Vol. 117, 2018, pp. 63–86.
11. Wickens, C. D., J. Helleberg, J. Goh, X. Xu, and W. Horrey. *Pilot Task Management: Testing an Attentional Expected Value Model of Visual Scanning*. UIUC Institute of Aviation Technical Report. University of Illinois, Savoy, November, 2001.
12. Werneke, J., and M. Vollrath. Where did the Car Come From? Attention Allocation at Intersections. *Proc., European Conference on Human Centred Design for Intelligent Transport Systems*, Berlin, Germany, 2010, pp. 197–206.
13. Denk, F., W. Huber, P. Brunner, and R. Kates. The Role of Perceptual Failure and Degrading Processes in Urban Traffic Accidents: A Stochastic Computational Model for Virtual Experiments. *Proc., 2020 IEEE 23rd International Conference on Intelligent Transportation Systems, ITSC 2020*, Rhodes, Greece, IEEE, New York, 2020.
14. Helmer, T. *Development of a Methodology for the Evaluation of Active Safety Using the Example of Preventive Pedestrian Protection*. Springer, Cham, 2014.
15. Rösener, C. *A Traffic-Based Method for Safety Impact Assessment of Road Vehicle Automation*. RWTH Aachen University, Germany, 2020.
16. Astarita, V., G. Guido, A. Vitale, and V. Giofré. A New Microsimulation Model for the Evaluation of Traffic Safety Performances. *European Transport – Trasporti Europei*, No. 51, 2012, pp. 1–16. <http://hdl.handle.net/10077/6117>.
17. Santhosh, D., B. K. Bindhu, and B. I. Koshy. Evaluation of Pedestrian Safety in Unsignalized T and X – Intersections Through Comparison of the Frequency and Severity of Pedestrian Conflicts. *Case Studies on Transport Policy*, Vol. 8, No. 4, 2020, pp. 1352–1359.
18. Khattak, A. J., N. Ahmad, B. Wali, and E. Dumbaugh. A Taxonomy of Driving Errors and Violations: Evidence From the Naturalistic Driving Study. *Accident Analysis and Prevention*, Vol. 151, 2021, p. 105873.
19. Gerstenberger, M. *Unfallgeschehen an Knotenpunkten - Grundlagenuntersuchung Zu Ursachen Und Ansätzen Zur Verbesserung Durch Assistenz*. Doctoral dissertation. Technische Universität München, Germany, 2015.
20. Müller, M., X. Longl, M. Betsch, D. Böhmmländer, and W. Utschick. Real-Time Crash Severity Estimation With

- Machine Learning and 2D Mass-Spring-Damper Model. *Proc., 2018 IEEE Conference on Intelligent Transportation Systems, ITSC*, Maui, HI, IEEE, New York, November, 2018, pp. 2036–2043.
21. TUM-VT. Ingolstadt Traffic Simulation in SUMO. https://github.com/TUM-VT/sumo_ingolstadt. Accessed November 29, 2021.
 22. Lopez, P. A., M. Behrisch, L. Bieker-Walz, J. Erdmann, Y. P. Flotterod, R. Hilbrich, L. Lucken, J. Rummel, P. Wagner, and E. Wiebner. Microscopic Traffic Simulation Using SUMO. *Proc., IEEE Conference on Intelligent Transportation Systems*, Maui, HI, IEEE, New York, 2018, pp. 2575–2582.
 23. Langer, M., M. Harth, L. Preitschaft, R. Kates, and K. Bogenberger. Calibration and Assessment of Urban Microscopic Traffic Simulation as an Environment for Testing of Automated Driving. *Proc., IEEE Intelligent Transportation Systems Conference*, Indianapolis, IN, IEEE, New York, 2021.
 24. Statistische Ämter des Bundes und der Länder. Unfallatlas. <https://www.govdata.de/dl-de/by-2->. Accessed July 27, 2021.
 25. GIDAS. German In-Depth Accident Study. <https://www.gidas.org>.
 26. Jurewicz, C., A. Sobhani, J. Woolley, J. Dutschke, and B. Corben. Exploration of Vehicle Impact Speed – Injury Severity Relationships for Application in Safer Road Design. *Transportation Research Procedia*, Vol. 14, 2016, pp. 4247–4256.
 27. Peng, Y., Y. Chen, J. Yang, D. Otte, and R. Willinger. A Study of Pedestrian and Bicyclist Exposure to Head Injury in Passenger Car Collisions Based on Accident Data and Simulations. *Safety Science*, Vol. 50, No. 9, 2012, pp. 1749–1759.
 28. Joksch, H. C.. Velocity Change and Fatality Risk in a Crash—A Rule of Thumb. *Accident Analysis & Prevention*, Vol. 25, No. 1, 1993, pp. 103–104.
 29. Müller, M., M. Botsch, D. Böhmländer, and W. Utschick. Machine Learning Based Prediction of Crash Severity Distributions for Mitigation Strategies. *Journal of Advances in Information Technology*, Vol. 9, No. 1, 2018, pp. 15–24.
 30. Böhmländer, D., T. Dirndorfer, A. H. Al-Bayatti, and T. Brandmeier. Context-Aware System for Pre-Triggering Irreversible Vehicle Safety Actuators. *Accident Analysis and Prevention*, Vol. 103, 2017, pp. 72–84.
 31. Funk, J. R., J. M. Cormier, and H. C. Gabler. Effect of Delta-V Errors in NASS on Frontal Crash Risk Calculations. *Annals of Advances in Automotive Medicine*, Vol. 52, 2008, pp. 155–164.
 32. Harth, M., M. Langer, and K. Bogenberger. Automated Calibration of Traffic Demand and Traffic Lights in SUMO Using Real-World Observations. *Proc., SUMO Conference*, Online, 2021.
 33. Gitelman, V., E. Doveh, and S. Bekhor. The Relationship Between Free-Flow Travel Speeds, Infrastructure Characteristics and Accidents, on Single-Carriageway Roads. *Transportation Research Procedia*, Vol. 25, 2017, pp. 2026–2043.
 34. Pei, X., S. C. Wong, and N. N. Sze. The Roles of Exposure and Speed in Road Safety Analysis. *Accident Analysis and Prevention*, Vol. 48, 2012, pp. 464–471.
 35. Imprialou, M. I. M., M. Quddus, D. E. Pitfield, and D. Lord. Re-Visiting Crash-Speed Relationships: A New Perspective in Crash Modelling. *Accident Analysis and Prevention*, Vol. 86, 2016, pp. 173–185.
 36. National Research Council. *Highway Capacity Manual*. US Department of Commerce, Washington, D.C., 2000.
 37. German Insurers Accident Research. *Unfalltypen-Katalog*. German Insurers Accident Research, 2016.
 38. Wang, C., M. A. Quddus, and S. G. Ison. Predicting Accident Frequency at Their Severity Levels and its Application in Site Ranking Using a Two-Stage Mixed Multivariate Model. *Accident Analysis and Prevention*, Vol. 43, No. 6, 2011, pp. 1979–1990.
 39. Gomes, S. V., S. R. Geedipally, and D. Lord. Estimating the Safety Performance of Urban Intersections in Lisbon, Portugal. *Safety Science*, Vol. 50, No. 9, 2012, pp. 1732–1739.
 40. Hauer, E., D. W. Harwood, F. M. Council, and M. S. Griffith. Estimating Safety by the Empirical Bayes Method: A Tutorial. *Transportation Research Record: Journal of the Transportation Research Board*, 2002. 1784: 126–131.
 41. Elvik, R. Comparative Analysis of Techniques for Identifying Locations of Hazardous Roads. *Transportation Research Record: Journal of the Transportation Research Board*, 2008. 2083: 72–75.
 42. Erdmann, J., and D. Krajzewicz. *SUMO's Road Intersection Model*. Springer-Verlag, Berlin, Heidelberg, 2011.
 43. Savino, G., M. Pierini, and N. Baldanzini. Decision Logic of an Active Braking System for Powered Two Wheelers. *Proceedings of the Institution of Mechanical Engineers, Part D: Journal of Automobile Engineering*, Vol. 226, No. 8, 2012, pp. 1026–1036.
 44. Green, M. “How Long Does it Take to Stop?” Methodological Analysis of Driver Perception-Brake Times. *Transportation Human Factors*, Vol. 2, No. 3, 2000, pp. 195–216.
 45. Idel, M. A Review of Matrix Scaling and Sinkhorn's Normal Form for Matrices and Positive Maps. *arXiv Preprint arXiv:1609.06349*, 2016, pp. 1–101.